Journal of Materials Research and Technology 35 (2025) 235–249

Contents lists available at ScienceDirect

Journal of Materials Research and Technology

journal homepage: www.elsevier.com/locate/jmrt

Graphene oxide and silver effects on the arc erosion properties of Al_2O_3–Cu/30Cr composite

Qiujie Liu [a], Meng Zhou [a,**], Baohong Tian [a,b,***], Yi Zhang [a,b,*], Qimeng Zhang [a], Jiacan Zhang [a], Zhiyu Han [a], Chunhe Chu [a], Ke Jing [a], Xu Li [c], Huiwen Guo [d], Alex A. Volinsky [e]

[a] School of Materials Science and Engineering, Henan University of Science and Technology, Provincial and Ministerial Co-construction of Collaborative Innovation Center for Non-ferrous Metals New Materials and Advanced Processing Technology, Luoyang, 471023, PR China
[b] Henan Province Key Laboratory of Nonferrous Materials Science and Processing Technology, Luoyang, 471023, PR China
[c] Center for Advanced Measurement Science, National Institute of Metrology, Beijing, 100029, PR China
[d] Chinalco Luoyang Copper Processing Co., Ltd., Luoyang, 471000, PR China
[e] Department of Mechanical Engineering, University of South Florida, 4202 E. Fowler, Ave. ENG 030, Tampa, 33620, USA

ARTICLE INFO

Handling editor: P Rios

Keywords:
Metal matrix composites
Copper matrix composites
Welding force
Contact resistance
Arc energy
Thermal stability

ABSTRACT

To investigate methods for enhancing the resistance of electrical contact materials to arc erosion, this study focuses on the preparation and properties of novel composites. Al_2O_3–Cu/30Cr and 0.3GO-0.3Ag/Al_2O_3–Cu/30Cr composites were fabricated using vacuum hot press sintering. The composites achieved high relative densities (99.82% and 99.6%), good electrical conductivities (47.8% IACS and 46.1% IACS), excellent hardness (142 HV and 158 HV), and superior thermal conductivities (124 W/(m·K) and 188 W/(m·K) at 150 °C), with compressive strengths of 693 MPa and 711 MPa. In addition, the addition of GO-Ag improved the resistance of the material to arc erosion, and the transfer and loss of the material were significantly reduced. Under the 30 V DC 30 A condition, the anode mass gain, cathode mass reduction and total mass loss decreasing from 3 mg, 3.73 mg, and 0.73 mg–1.97 mg, 2.30 mg, and 0.33 mg, respectively. Furthermore, the transmission electron microscopy (TEM) and energy dispersive spectrometer (EDS) results show that Cr_3C_2 compounds effectively pin the Cr–Cu interface. High thermal conductivity and good micro-interface improve the electrical contact properties of the composites and help to improve the compression properties.

1. Introduction

Metal Matrix Composites (MMCs) are a combination of metal matrix materials and reinforcement. By selecting different reinforcement phases and appropriate preparation methods [1,2], the strength, hardness, and other properties of metal matrix composites can be significantly improved, so as to be widely used in aerospace, automotive, and electronic fields [3,4].

Copper matrix composites are ideal for high performance electronic components and electrical connections due to their excellent electrical and thermal conductivity. Dispersion strengthened copper matrix composite is a kind of composite material that introduces fine dispersed phase particles into the copper matrix so that the strength of the matrix, especially the high temperature strength, can be greatly improved. Common dispersion strengthening materials include Al_2O_3 [5,6], Y_2O_3 [7], ZrO_2 [8–10], and so on, which help refine grains, improve density, and enhance mechanical properties. Among these, nano-Al_2O_3 particles produced by the internal oxidation are particularly effective due to their thermal stability and strength [11]. Tian et al. [12] prepared Cu-0.5% Al_2O_3 composites by internal oxidation method with high electrical conductivity, softening temperature, and yield strength up to 93% IACS, 800 °C, and 169 MPa, respectively. This is due to the fact that Al_2O_3 nanoparticles pinning dislocations inhibit the recrystallization of the material, and thus the integrated performance of the material is greatly

* Corresponding author. School of Materials Science and Engineering, Henan University of Science and Technology, Provincial and Ministerial Co-construction of Collaborative Innovation Center for Non-ferrous Metals New Materials and Advanced Processing Technology, Luoyang, 471023, PR China.
** Corresponding author.zhoumeng0902@126.com
*** Corresponding author. School of Materials Science and Engineering, Henan University of Science and Technology, Provincial and Ministerial Co-construction of Collaborative Innovation Center for Non-ferrous Metals New Materials and Advanced Processing Technology, Luoyang, 471023, PR China.bhtian007@163.com
E-mail address: zhshgu436@163.com (Y. Zhang).

https://doi.org/10.1016/j.jmrt.2025.01.007
Received 6 November 2024; Received in revised form 28 December 2024; Accepted 3 January 2025
Available online 4 January 2025

improved. To further improve the mechanical properties and thermal stability of materials, graphene (Gr) is a highly effective reinforcement for metal matrix composites [13]. However, poor wettability between the Cu matrix and Gr often leads to agglomeration. Graphene oxide (GO) helps solve this issue, and under high temperatures, GO is reduced to reduced graphene oxide (RGO), resulting in restoring the structure of Gr and improving material performance. Luo et al. [14] reinforced copper composites with Ag-modified RGO using vacuum hot press sintering, showing that 1.6 vol% Ag-RGO had the best corrosion resistance. Chu et al. [15] added RGO to Cu–Cr composites and found that Cr_7C_3 at the interface improved bonding, heat resistance, and mechanical properties. Nazeer et al. [16] used powder metallurgy to prepare Cu-RGO composites and showed that 0.5 wt% GO significantly improved tensile strength, ductility, thermal conductivity, and hardness. These studies suggest that the right amount of GO significantly enhances composite performance. This lays the foundation for its application in the field of electrical contacts. Through the use of different reinforcement materials, such as ceramic particles, graphene, etc., the mechanical properties and thermal stability of copper matrix composites have been effectively improved.

Electrical contact materials are materials used for electrical connection and exchange, which are required to have excellent properties in temperature rise, arc erosion resistance, and fusion welding resistance. To ensure the safety and stability of electrical contact materials in switches, relays, circuit breakers, and other electrical equipment [17–19]. This requires that the electrical contact material itself must have high electrical and thermal conductivity, arc erosion resistance and stable contact resistance [20–24]. Copper matrix composites are favored because of their excellent electrical conductivity and wear resistance. Thus, developing new vacuum contact materials is essential to meet these urgent requirements. Recently, copper-based electrical contact material systems mainly include Cu-Cr [25,26], Cu–W [27], and Cu–Mo [28] systems. The Cu–Cr system is especially notable due to chromium's properties, such as high melting point, hardness, and low solubility in copper, which enhance resistance to arc erosion [29]. Inada et al. [30] investigated the relationship between two-dimensional electron and metal vapor density distributions and chromium content over a vacuum arc generated between Cu–Cr electrodes, it found that vacuum arc performance was improved when Cr content is between 25 wt% and 35 wt%. Papillon et al. [31] prepared Cu–Cr alloys by powder metallurgy and showed that Cr reacts with oxygen during sintering, reducing alloy expansion and creating a denser Cu–Cr material, enhancing the high arc-breaking capacity. Thus, the addition of chromium has a significant effect on sintering densification and arc-breaking ability. Zhu et al. [32] also found nano-Al_2O_3 particles improved the mechanical properties and arc resistance of composites. To optimize electrical conductivity and strength, silver (Ag) is often added to copper matrix composites due to its superior conductivity. Güler O et al. [33,34] prepared Al_2O_3 reinforced copper matrix composites by electroless plating and hot pressing, and showed that Ag had a positive effect on the conductivity and oxidation resistance of the composite. Ma et al. [35] found that Ag reduced resistivity in composites, and Zhou et al. [36] showed that adding Ag to Cu–Al_2O_3 refined the structure and improved both conductivity and strength. The combination of nano-Al_2O_3 and Ag effectively enhances the overall performance of copper matrix composites, improving electrical contact properties. The above research shows that by optimizing the material combination and preparation process, the overall performance of electrical contact materials can be significantly improved to meet the needs of high load and high frequency applications.

Based on previous research, this study aims to design and investigate two novel composites: Al_2O_3–Cu/30Cr and 0.3GO-0.3Ag/Al_2O_3–Cu/30Cr. Using Al_2O_3–Cu/30Cr as the matrix and trace amounts of Ag and GO as reinforcing phases, the composites were synthesized via vacuum hot-press sintering and internal oxidation. The comprehensive performance and microstructure were characterized, and the electrical erosion properties were studied. The effects of Ag and GO on dispersed Al_2O_3–Cu/30Cr composites were studied in this work, which provides valuable insights and a theoretical basis for the development of electric contact materials.

2. Experimental materials and methods

2.1. Preparation of composite materials

The pristine materials used in the experiment included Cu-0.35 wt% Al alloy powder (average particle size 37 μm), Cu_2O powder (1–5 μm), Cr powder (10 μm), Ag powder (3 μm), and GO (average thickness 0.8–1.2 nm, sheet diameter 0.5–5 μm). All raw materials had a purity greater than 99.9%. Table 1 details the composition ratios required for the composites, while Fig. 1 illustrates the composite preparation process.

The Cu-0.35 wt% Al alloy, Cu_2O, Cr, Ag powders, and GO were weighed according to the specified ratios and loaded into a homemade plastic ball milling jar, which contained zinc-copper balls with diameters of 5 mm and 3 mm in a 2:1 ratio, with a ball material ratio of 5:1. The sealed jars were ground for 6 h in a roller ball mill at 65 r/min.

After milling, the composite powder was loaded into 30 mm cylindrical graphite molds and initially compacted using a small hydraulic press. The molds were then placed in a rapid hot press sintering furnace. The furnace operated at a heating rate of 100 °C/min, starting with a pressure of 35 MPa. The second heating stage reached 700 °C for 3 min, followed by a third stage at 950 °C for 15 min at 45 MPa. The process then included cooling and pressure reduction: the temperature decreased to 500 °C, the pressure to 25 MPa, and the vacuum in the furnace was maintained below 3 Pa. After completing the program, pressure was released, and the specimen was allowed to cool with the furnace to below 150 °C before removal.

2.2. Performance testing of composite materials

The two end surfaces of the sintered (GO, Ag)/Al_2O_3–Cu/30Cr composites were sandpapered to achieve a smooth finish. A polishing machine was then used to ensure that the surfaces were free of oxidation, pits, or scratches before testing the composite material for its basic properties.

The conductivity of the sintered composites was measured according to ASTM B193-16 using a Sigma2008B1 digital conductivity tester, with measurements taken at 10 evenly spaced locations along the diameter for averaging. The actual density was first determined in accordance with ASTM B311-22, and the relative density was calculated as the ratio of actual density to theoretical density. Vickers hardness was measured using the HVS-1000 microhardness tester per ASTM B384-17, applying a load of 500 g for 10 s, with an average of 8 measurements per sample.

Room temperature compression tests were conducted following ASTM E9-19 standards using a Shimadzu AGI-250 kN universal testing machine, with three samples prepared for each specimen. The sintered composite specimens were wire-cut into cylindrical standard samples (Φ12.5 mm × 2.5 mm) for thermal conductivity analysis, performed with an LINSEIS LFA 500 Laser thermal conductivity measuring instrument at 25 °C and 150 °C and a ramp rate of 5 °C/min, averaging three measurements for each specimen. The instrument was calibrated with a quartz rod, and argon was used as a protective gas during testing.

Table 1
Composition of (GO, Ag)/Al_2O_3–Cu/Cr composites (wt.%).

Composites	Cu-0.35 wt% Al	Cr	Cu_2O	Ag	GO
Al_2O_3–Cu/30Cr	66.7	30	3.3	/	/
0.3GO-0.3Ag/Al_2O_3–Cu/30Cr	66.1	30	3.3	0.3	0.3

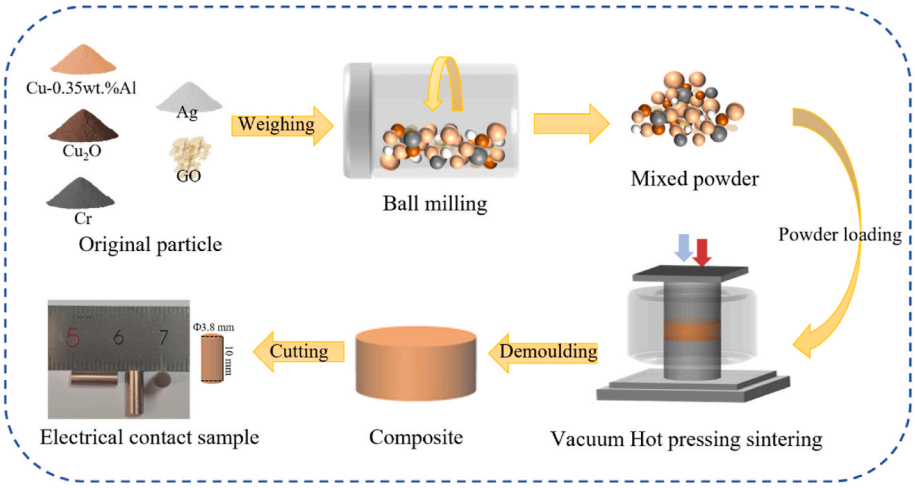

Fig. 1. Schematic diagram of the composite materials preparation.

2.3. Electrical contact experiments

The two end surfaces of the cylindrical specimen (Φ3.8 mm × 10 mm) of the electrical contact were ground until smooth and then polished. The JF04C electrical contact test system was used for testing, and its testing process was protected by argon gas, as shown in Fig. 2. The anode is the moving contact, and the cathode is the static contact. Contact opening and closing for a test, the number of tests is 5000 times. The mass of each electrical contact before and after the test is m_1 and m_2, respectively, weighed with an analytical balance with an accuracy of 0.1 mg, and the mass difference ($\Delta m = m_2\text{-}m_1$) is calculated as the basis for mass transfer. The test parameters are DC 30V, 10A, 20A, 25A, 30A, the frequency of splitting and closing is 60 times/min, and the range of dynamic and static contact closing pressures is controlled between 0.40 N and 0.60 N. The welding force, contact resistance, arc energy, and other data of the testing process are monitored in real time.

2.4. Microstructure characterization

The crystal structures of the original powder and sintered state composites were analyzed using D8-advanced X. And the surface morphology of the composites in powder state, sintered state, and after arc erosion were observed and analyzed using the JSM-IT100 scanning electron microscope. The surfaces of the specimens in the sintered state and after arc erosion were analyzed by EDS energy spectroscopy using the JSM-7800F field emission scanning electron microscope. The three-dimensional surface image of the specimen was obtained with the PA53MET-3D high depth-of-field optical microscope. And the microstructure of the samples was examined using the Zeiss LIBRA-200FE transmission electron microscope.

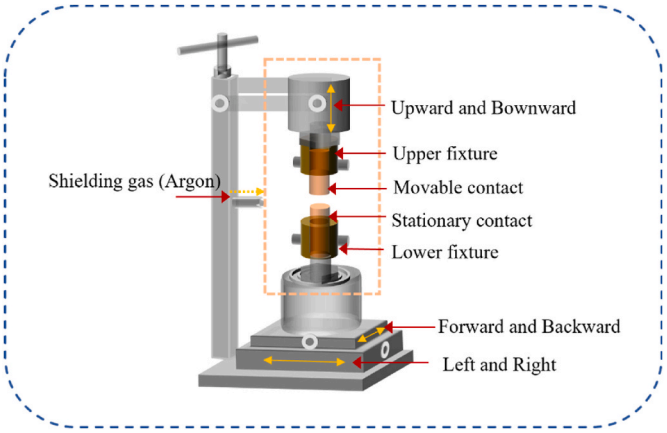

Fig. 2. JF04C contact material testing system schematic diagram.

3. Results

3.1. Microstructure and integrated properties of composite materials

Fig. 3 shows the SEM of the pristine powder of the prepared composite. Fig. 3(a–d) show the morphology of different phase powders. And the morphologies of two composites mixed powders can be seen from Fig. 3(e and f), which are the composite powders of Al_2O_3–Cu/30Cr and 0.3GO-0.3Ag/Al_2O_3–Cu/30Cr composites. Various powders were mixed uniformly, and there was no obvious agglomeration of powder. Thus, it is indicated that the reinforcement phases uniformly distribute in matrix during sintering process.

Fig. 4 shows the SEM images and EDS results of Al_2O_3–Cu/30Cr and 0.3GO-0.3Ag/Al_2O_3–Cu/30Cr composites. Uniform distribution of each phase for both composites can be observed in Fig. 4(a and b). Fig. 4(c) shows the point-scan and surface-scan images of the Al_2O_3–Cu/30Cr composite, which shows that the boundary between the Cu matrix and the second reinforcing phase Cr particles is clear, and no Al_2O_3-enriched area is found; the line scan of the 0.3GO-0.3Ag/Al_2O_3–Cu/30Cr composite is shown in Fig. 4(d), which shows that there exists a certain degree of mutual solubility of the reinforcing phase Cr and the Cu matrix.

Fig. 5 shows the X-ray diffraction (XRD) scans of Al_2O_3–Cu/30Cr and 0.3GO-0.3Ag/Al_2O_3–Cu/30Cr composites. In Fig. 5(a), four diffraction peaks with 2θ = 43.3°, 50.4°, 74.1°, and 89.9°(PDF#04–0836) were detected within the scanning angle of 25°–95° corresponding to the (111), (200), (220), and (311) crystal planes of Cu, respectively. The three diffraction peaks at 2θ = 44.3°, 64.6° and 81.7°(PDF#06–0694) correspond to the (110), (200), (220) and (211) crystal planes of Cr, respectively. Compared with Fig. 5(a), the (111) (PDF#74–1230) crystal plane of Cu_2O in the small diffraction peak fraction of the composite powder disappears in Fig. 5(b). It indicates that the internal oxidation occurs in the sintering process, and the related chemical reactions are shown in Equation (1) (2) (3) [37].

$$2CuO = 2Cu + 1/2O_2 \quad (1)$$

$$Cu_2O = 2Cu + 1/2O_2 \quad (2)$$

$$2Al + 3/2O_2 = Al_2O_3 \quad (3)$$

Due to the small amount of Ag and GO addition, and the low content of Al_2O_3 generated by internal oxidation, their diffraction peaks were

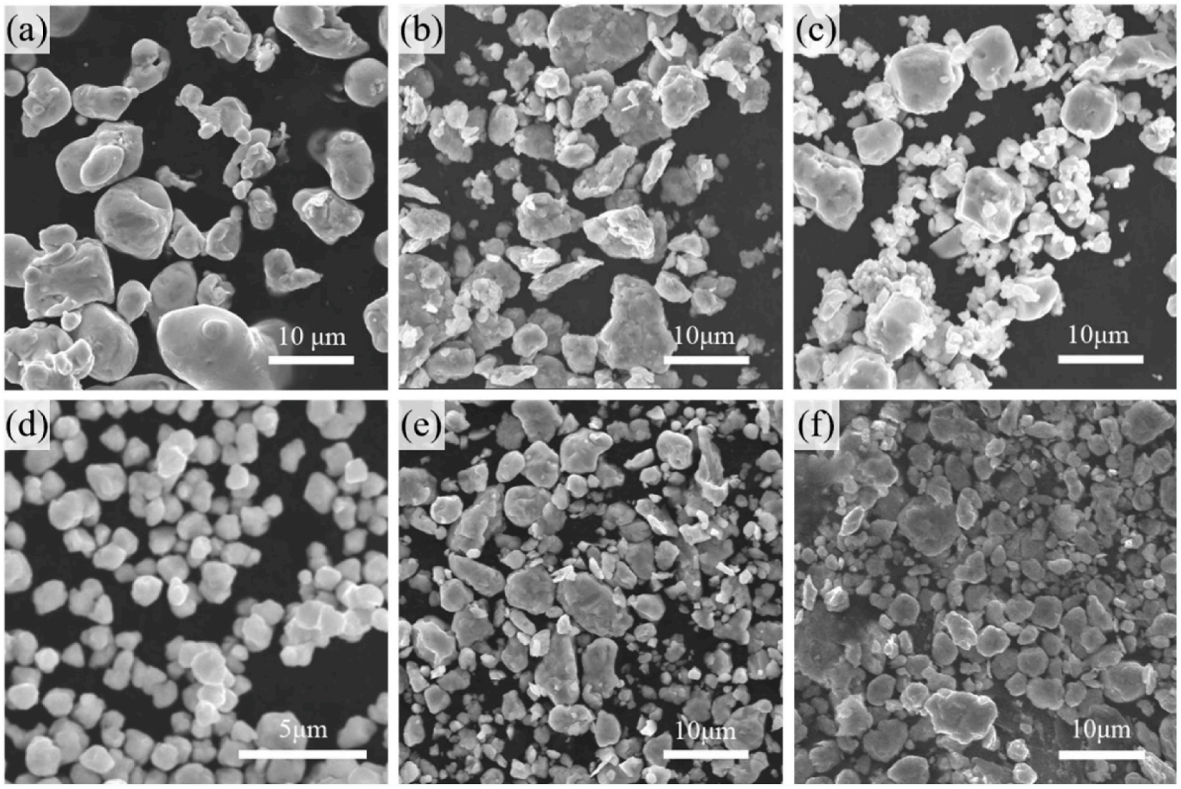

Fig. 3. SEM images of the different powders: (a) Cu-0.35 wt % Al; (b) Cr; (c) Cu_2O; (d)Ag; (e) Al_2O_3–Cu/30Cr composite; (f) 0.3GO-0.3Ag/Al_2O_3–Cu/30Cr composite.

not scanned. And no miscellaneous peaks such as oxides were detected from the XRD spectra, indicating that the raw materials were not oxidized by contamination.

The comprehensive properties of (GO, Ag)/Al_2O_3–Cu/Cr composites are shown in Table 2. The relative densities of both Al_2O_3–Cu/30Cr and 0.3GO-0.3Ag/Al_2O_3–Cu/30Cr were above 99%. And the latter shows a slight decrease in the electrical conductivity of the composites compared to the former. However, the compressive strength and hardness were improved by 2.6% and 7.3% respectively. and thermal conductivity of the composites is increased by 26.1% at 25 °C and 51.6% at 150 °C with the addition of Ag and GO, respectively.

Although the electrical conductivity of Ag is higher than that of Cu, the addition of trace amounts of Ag to the composites enhances the electron scattering at the interface between the matrix, which leads to a decrease in the electrical conductivity. In addition, the added GO was reduced to R-GO at high temperatures. It provides C and then C combine with Cr to produce Cr–C compounds in the matrix, resulting in lattice distortion. It caused stress concentration and enhanced scattering of electrons, leading to a decrease in the electrical conductivity, but the resulting Cr–C compounds pinned dislocations and form dislocation packages, which impeded the dislocation motion and improve the strength and hardness of the material.

Wang et al. [38] investigated G/Cu composites with different graphene contents and showed that graphene improved the thermal and electrical conductivity of the composites. The thermal conductivities of silver and copper were 429 W/(m·K) and 401 W/(m·K), respectively. The thermal conductivity of the added elements is higher than that of the copper matrix, and the experimental results show that the thermal conductivity of the composites is increased by 26.1% at 25 °C and 51.6% at 150 °C with the addition of Ag and GO, respectively. It shows that the thermal conductivity is very sensitive to the temperature. It is generally believed that the electrical conductivity is consistent with the thermal conductivity, but in this experiment, the addition of a trace amount of Ag solid-solved in the matrix has a small effect on the electrical conductivity enhancement and the formation of impurity defects enhances the thermal resistance, which will reduce the thermal conductivity. However, Akbari et al. [39] suggested that the thermal conductivity of the heat-treated and pressed GO surface is 2025 W/(m·K). The added GO is R-GO after internal reduction to restore the properties of Gr. It was shown that the thermal conductivity of Gr is as high as 5000 W/(m·K) [40]. Therefore, the enhancement of thermal conductivity by R-GO is much greater than the reduction of Ag and plays a dominant role in the overall thermal conductivity improvement of the composites.

3.2. Transfer of substances

Fig. 6 shows the mass transfer of each pair of cathode-anode contacts of both composites before and after 5000 times tests at different currents. It can be seen that as the current increases, the anode mass gradually increases and the cathode mass gradually decreases. However, the decrease in cathode mass is higher than the increase in anode mass. It shows that the mass transfer of both composites is from cathode to anode, and part of it was lost in the environment, and the mass transfer and loss of cathode and anode contacts are gradually increasing with the increase of current. When the current is much more 10 A, it can be seen that the addition of trace amounts of GO and Ag significantly reduces the mass transfer and loss of contact material. In particular, the anode mass increase, cathode mass decrease and total mass loss of 0.3GO-0.3Ag/Al_2O_3–Cu/30Cr composites were reduced by 34.3%, 38.3% and 54.8%, respectively, when compared with Al_2O_3–Cu/30Cr at a current of 30 A.

The mass change results indicate that erosion and transfer of contact material occurred during electrical contact. The cathode material transfer is mainly affected by the combined effects of arc transfer, liquid bridge transfer, oxidation weight gain, material vaporization. At a current of 10 A, the current density is low, and the gasification temperature is not reached, so mass transfer mainly occurs through arc transfer and oxidation. When the current increases 20–30 A, the arc energy increases,

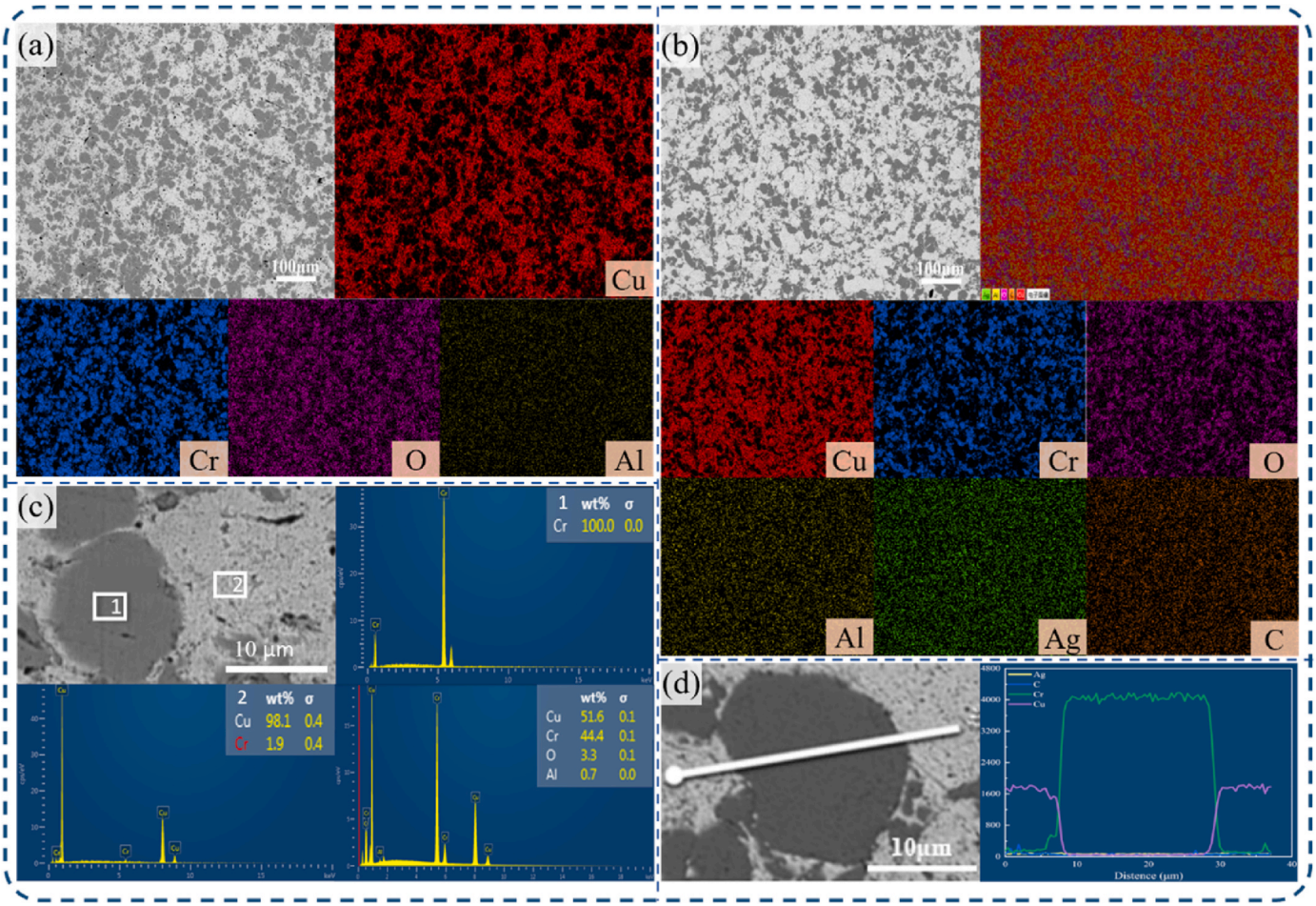

Fig. 4. SEM images and EDS results of composites: (a, c) Al_2O_3–Cu/30Cr composite; (b, d) 0.3GO-0.3Ag/Al_2O_3–Cu/30Cr composite.

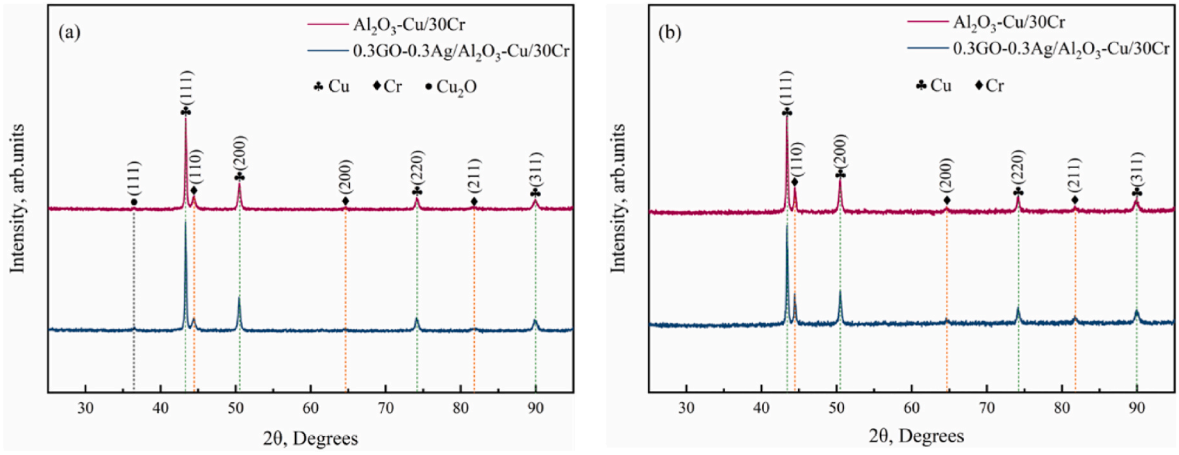

Fig. 5. XRD spectrum of two composites: (a) composite powder; (b) composite sintered state.

Table 2
Comprehensive properties of (GO, Ag)/Cu–Al_2O_3/Cr composites.

Composites	Relative Density %	Electrical conductivity %IACS	Vickers hardness $HV_{0.5}$	Thermal conductivity W/(m·K)		Compressive strength MPa
				25 °C	150 °C	
Cu–Al_2O_3/30Cr	99.82	47.8	142	176	124	693
0.3GO-0.3Ag/Al_2O_3–Cu/30Cr	99.60	46.1	158	222	188	711

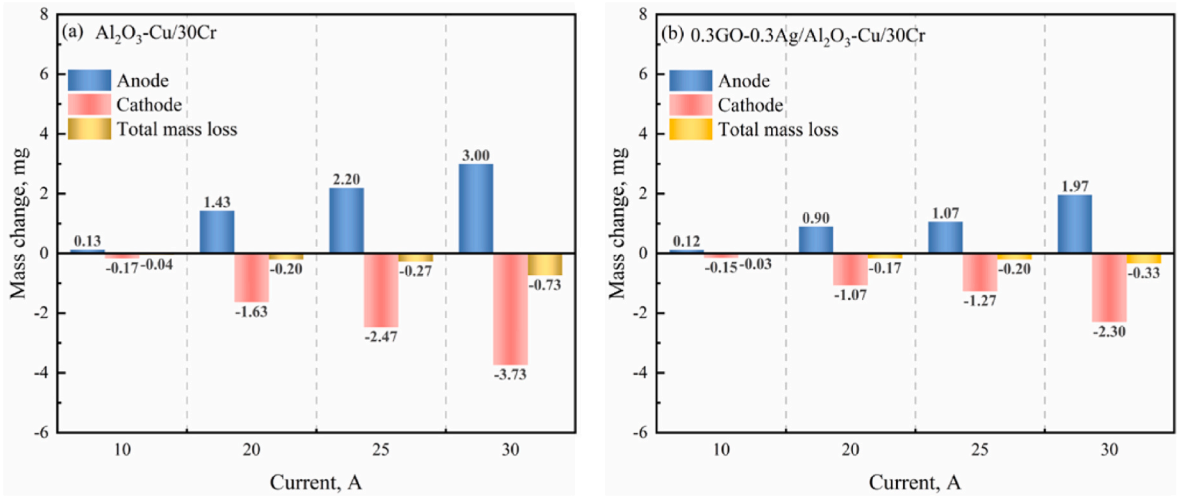

Fig. 6. The result of mass transfer after arc erosion: (a) Al_2O_3–Cu/30Cr; (b) 0.3GO-0.3Ag/Al_2O_3–Cu/30Cr.

and the surface temperature rises rapidly due to the Cu matrix on the contact surface to melt and evaporate. Upon disconnection, the liquid bridges break unevenly, leading to mass transfer. As the current increases, the extent of mass transfer also rises.

Arc transfer refers to the movement of metal atoms from the cathode to the anode along the direction of electron flow in a high-current-density arc, explaining the consistent mass transfer from the cathode to the anode. When the current was 30 A, the mass changes result from the combined effects of arc transfer, liquid bridge formation, vaporization, and oxidation.

For the 0.3GO-0.3Ag/Al_2O_3–Cu/30Cr composites, the solid solution of Ag and the formation of Cr–C compounds were occurred due to the

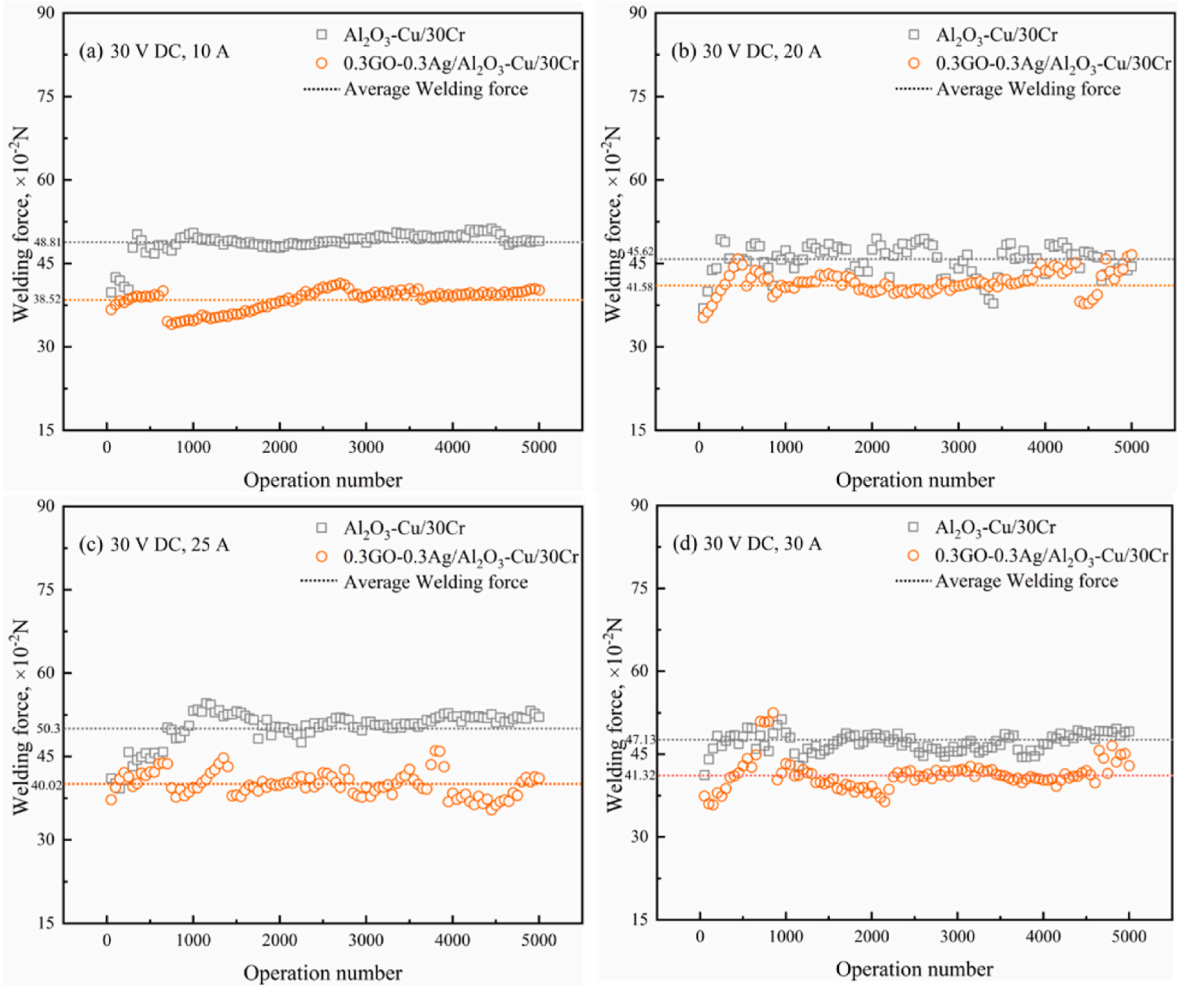

Fig. 7. The relationship of the welding force to the operation numbers: (a) 30 V DC,10 A; (b) 30 V DC,20 A; (c) 30 V DC, 25 A; (d) 30 V DC, 30 A.

incorporation of GO and Ag, which enhances the mechanical properties of the materials while improving the high temperature stability, reduces the mechanical wear of the composites as well as the degree of melting at high temperatures, and reduces the spattering of the metal droplets, which reduces the mass transfer and the loss of the materials.

3.3. Welding force

Fig. 7 illustrates the variation of the welding force of the two composites at different currents during the 5000 times electrical contact tests. Each point represents the average value of 100 breaking operations. As can be seen in Fig. 7(a–d), the welding force of the two materials fluctuates above and below the mean value with the increase of the number of tests, and the welding force of the 0.3GO-0.3Ag/Al_2O_3–Cu/30Cr contacts is relatively low and more stable. Among them, the addition of Ag and GO decreased the average welding force by 21.1% and 20.4% when the current was 10 A and 25 A, respectively.

The reason for this phenomenon is that as the current rises, a large amount of Joule heat is released, thus melting the metal on the surface of the contacts, and the welding force is generated when the molten layer of the two contacts cools increases. As the contact position inevitably shifts during contact, the contact area of the two contacts varies greatly due to the severely erosion of the sample surface. When the contact position is the tip produced by erosion, the contact area decreases, and the current density increases, more Joule heat is produced, plastic deformation was occurred under the action of the externally applied force resulting in severe adhesion. It is the high degree of difference in erosion surface morphology that causes the welding force to fluctuate. However, the addition of GO and Ag to the contact materials improved the high temperature stability properties of the materials, and the erosion surface was relatively flat with better disconnecting ability, which improved the anti-melt welding performance of the contact materials.

3.4. Contact resistance

Fig. 8 shows the relationship of the contact resistance to the operation numbers of Al_2O_3–Cu/30Cr and 0.3GO-0.3Ag/Al_2O_3–Cu/30Cr composites under 30 V DC, 10–30 A. At a constant voltage of 30 V, the contact resistance of the Al_2O_3–Cu/30Cr and 0.3GO-0.3Ag/Al_2O_3–Cu/30Cr decreased gradually with the increase of current during the electrical contact tests. In Fig. 8(a), at low current, the contact resistance of the Al_2O_3–Cu/30Cr contact shows a trend of decreasing and then increasing followed by a flat region. Although the average contact resistance is lower than that of the 0.3GO-0.3Ag/Al_2O_3–Cu/30Cr contact, the fluctuation of the contact resistance is large. In Fig. 8(b and c), the average values of contact resistance of 0.3GO-0.3Ag/Al_2O_3–Cu/30Cr contacts at currents of 20 A and 25 A are relatively low. In Fig. 8(d), the difference between the contact resistance of the two materials is very small when the current is 30 A. Generally, the contact resistance of the 0.3GO-0.3Ag/Al_2O_3–Cu/30Cr contacts is much lower and stable. This is because the contact resistance of the contact material is related to the oxidation resistance of the contact interface, as well as the stability of the oxide film. The addition of GO and Ag improves the oxidation resistance of the material, thus it less likely to oxidize and the oxide film to rupture in the contact process. At low current, the 0.3GO-0.3Ag/

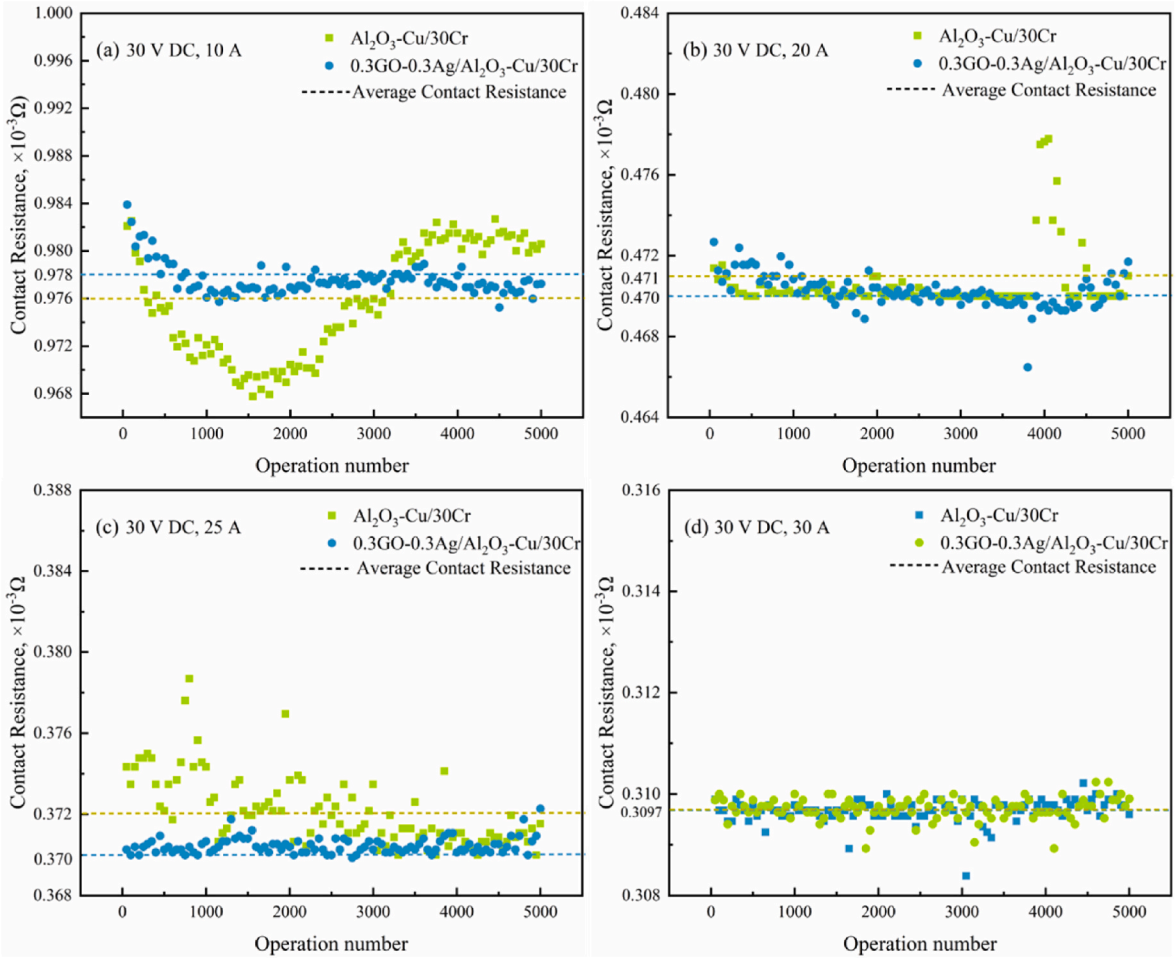

Fig. 8. The relationship of the contact resistance to the operation numbers: (a) 30 V DC, 10 A; (b) 30 V DC, 20 A; (c) 30 V DC, 25 A; (d) 30 V DC, 30 A.

Al_2O_3–Cu/30Cr contact material plays a more obvious role on the contact resistance, and the contact resistance shows low and stable; at high current 30 A, due to the extremely high energy of the arc, the oxide film is seriously damaged, and the test parameter plays a dominant role on the contact resistance, that is to say, under the same parameter, there is not much difference in the contact resistance of the two materials at high current.

3.5. Arc energy and arc duration

The arc energy and arc duration can reflect the arc extinguishing ability of the material. The smaller of arc energy and the shorter of arc duration, the stronger of arc extinguishing ability of the material [41, 42]. It can be seen in Fig. 9(a and b) that the average arc energy and average arc duration for both materials increase with increasing current. Under the same test conditions, the average arc energy and average arc duration of 0.3GO-0.3Ag/Al_2O_3–Cu/30Cr contact materials were significantly lower than those of Al_2O_3–Cu/30Cr. At a current of 30 A, the average arc energy and average arc duration of the 0.3GO-0.3Ag/Al_2O_3–Cu/30Cr contact material were 16.8% and 12.7% lower than those of the Al_2O_3–Cu/30Cr contact material, respectively.

Fig. 10 exemplifies the variation of arc energy and arc duration for two contact materials at currents of 10 A and 30 A. It can be seen that the current increases, the arc energy of the two materials is increased. The arc energy of the 0.3GO-0.3Ag/Al_2O_3–Cu/30Cr contact material is low and stable under the same test parameters.

4. Discussion

4.1. Relationship between arc duration and arc energy

It can be seen that the arc duration and arc energy of the two materials have similar trends from Fig. 10. In order to specifically explore the relationship between arc energy and arc duration, the linear fitting of the arc duration versus arc energy for Al_2O_3–Cu/30Cr and 0.3GO-0.3Ag/Al_2O_3–Cu/30Cr under the test condition of 30 V DC, 30 A was carried out as shown in Fig. 11. From the figure, it can be seen that arc energy and arc duration are linearly related, and the degree of correlation is greater than 0.99, and the fitting equations obtained are as follows:

$$E_1 = 116.96t+25.21\ R^2 = 0.997 \quad (4)$$

$$E_2 = 117.33t+43.78\ R^2 = 0.996 \quad (5)$$

According to the above equations, the point of intersection T = -50.18 < 0, since $k_2 > k_1$, (k_1, k_2 are the slopes of E_1, E_2 respectively), so the equation E_2 is always above E_1 when T > −50.18, which means is T ≥ 0. That is to say, the composite 0.3GO-0.3Ag/Al_2O_3–Cu/30Cr has a shorter arc duration when $E_1 = E_2$ under 30 V DC, 30 A (T ≥ 0) test conditions. When the arc energy E = 500 mJ, 1000 mJ, 1500 mJ, the composites Al_2O_3–Cu/30Cr and 0.3GO-0.3Ag/Al_2O_3–Cu/30Cr at 30 V DC, 30 A correspond to the arc duration T_1 and T_2, respectively, and the calculations are listed in Table 3, and the arc duration after the addition of GO and Ag decreases by 4.0%, 2.3% and 1.6%, respectively. It is shown that 0.3GO-0.3Ag/Al_2O_3–Cu/30Cr and Al_2O_3–Cu/30Cr are comparable in their ability to inhibit the arc duration at 30 V DC, 30 A when the arc energy is constant.

4.2. Arc erosion mechanism

In order to further analyze the variation mechanism of the mass of the electrical contact materials, the surfaces of the two composites were characterized by SEM after 30 V DC, 30 A electrical erosion, as shown in Fig. 12. The anodes of both composites mainly exhibit a raised shape and the cathodes mainly exhibit a concave shape. Fig. 13 shows the 3D morphology of the contact surface after erosion under this experimental condition. As shown in Fig. 13(a–c), the height difference corresponding to the anode and cathode of the Al_2O_3–Cu/30Cr composite after arc erosion is 164 μm and 102 μm, respectively, whereas in Fig. 13(b–d), the height difference corresponding to the anode and cathode of the 0.3GO-0.3Ag/Al_2O_3–Cu/30Cr composite after arc erosion is 97 μm and 67 μm, respectively. The 0.3GO-0.3Ag/Al_2O_3–Cu/30Cr composites showed better resistance to arc erosion at the same voltage and current.

Fig. 14 shows the SEM images of the two composites after arc erosion. Typical electrical erosion morphologies can be seen for both composites, such as drop, humps, pits, cracks, pores, skeletons, coral structures, etc. The Al_2O_3–Cu/30Cr composite has fragments and relatively wide microscopic cracks compared with the morphologies of the 0.3GO-0.3Ag/Al_2O_3–Cu/30Cr. In addition, the skeleton structure of Al_2O_3–Cu/30Cr is relatively less, which indicates that the addition of trace amounts of Ag and GO largely improves the arc erosion resistance. The inputting of the arc heat increases the temperature of the contacts. Consequently, it forms a regional melting melt layer area.

The copper matrix melts first, and spherical droplets are formed by splashing during the contact opening and closing process. With the extremely fast cooling rate, the liquid metal solidifies during the spreading process, and the spreading droplets are formed. And the result is an uneven surface in the molten layer. Cracks are produced by rapid cooling contraction of the molten liquid metal, as shown in Fig. 14(a). Many coral-like morphologies can be observed at the edges of the eroded

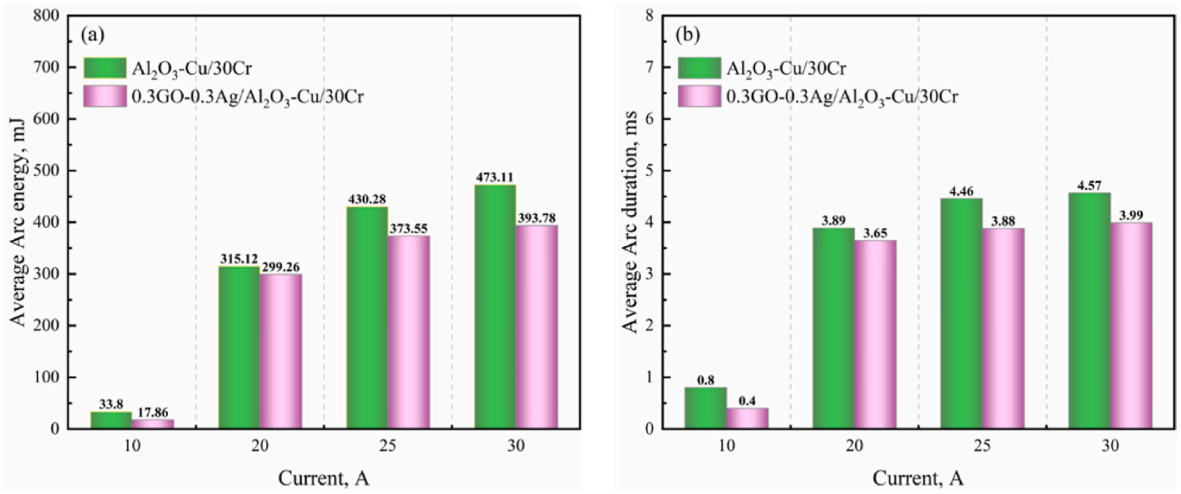

Fig. 9. Arc property under different currents: (a) average arc energy; (b) average arc duration.

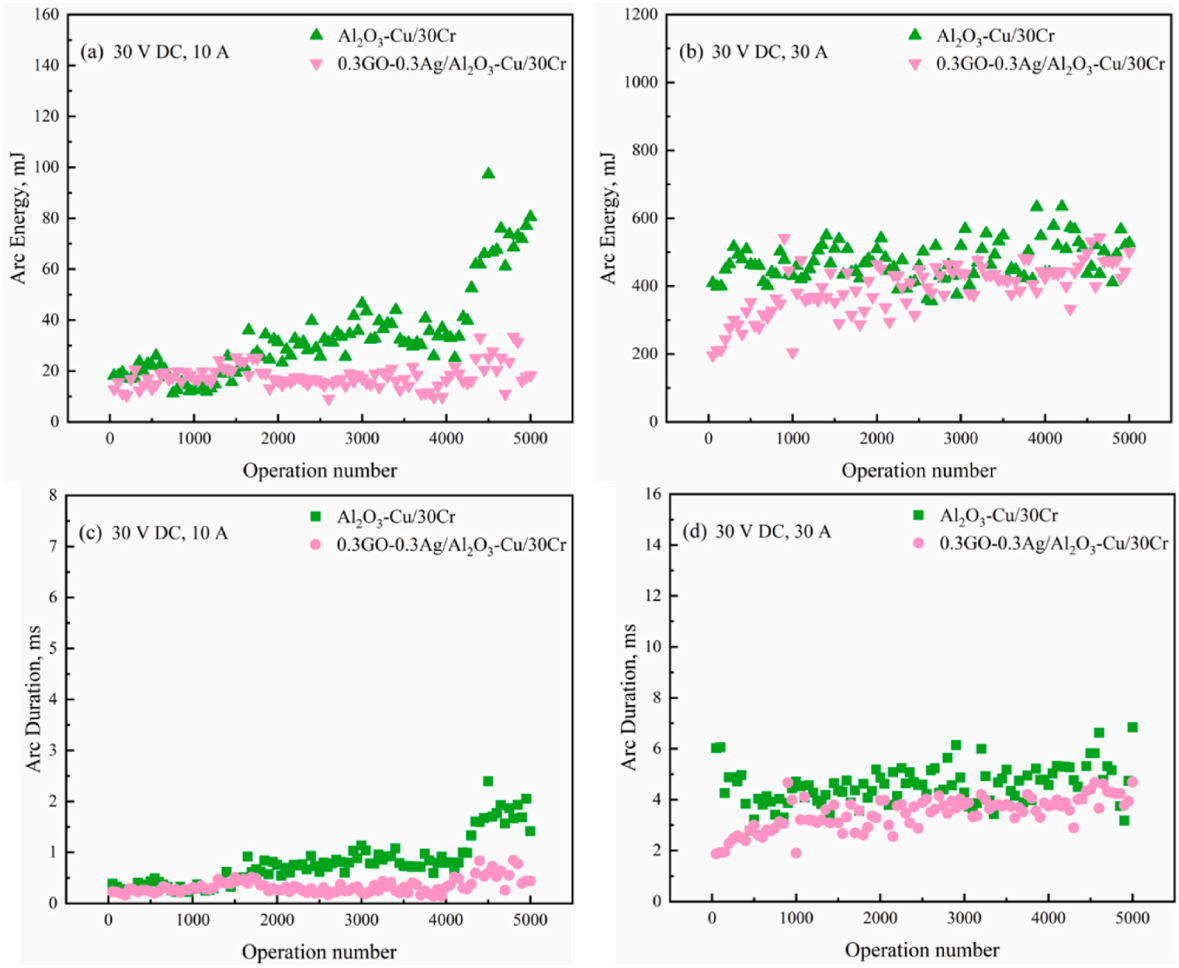

Fig. 10. Arc energy vs arc duration at 30 V DC, 10 A and 30 V DC, 30 A: (a, c) Al_2O_3–Cu/30Cr; (b, d) 0.3GO-0.3Ag/Al_2O_3–Cu/30Cr.

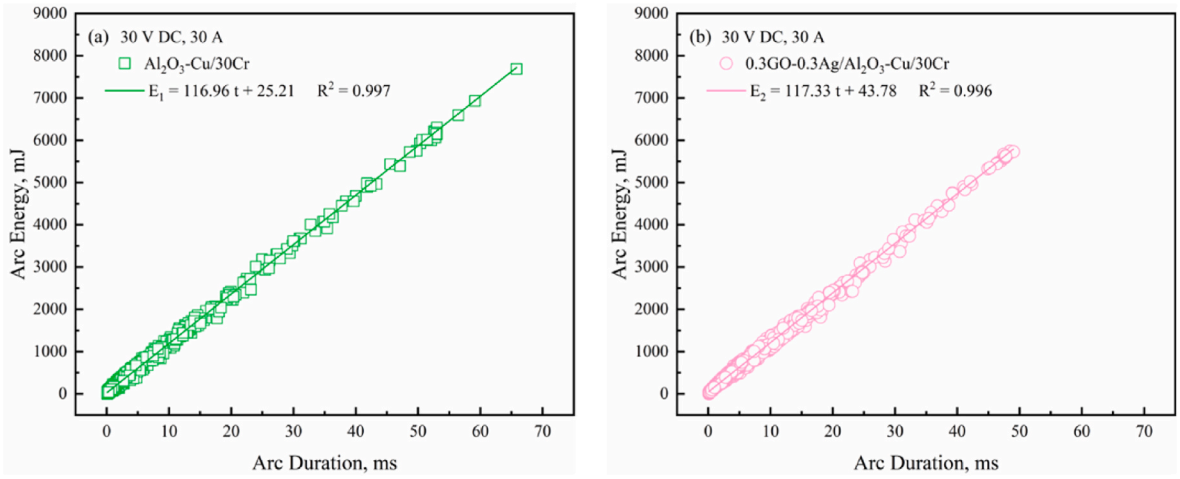

Fig. 11. Arc energy vs arc duration at 30 V DC, 30 A: (a) Al_2O_3–Cu/30Cr; (b) 0.3GO-0.3Ag/Al_2O_3–Cu/30Cr.

Table 3
Arc duration corresponding to different arc energy of two materials.

Arc Energy, mJ	T_1, ms	T_2, ms
500	4.05	3.89
1000	8.33	8.14
1500	12.61	12.41

areas, formed due to the oxidation of the sputtered liquid metal during the low-temperature cooling process at the edges. The formation of air holes is due to the overheating and melting of the substrate copper under the action of the electric arc, the liquid copper has a higher solubility for oxygen compared to the solid copper and absorbs a large amount of O_2 from the air, and a chemical reaction occurs at high temperatures by following equation [43]:

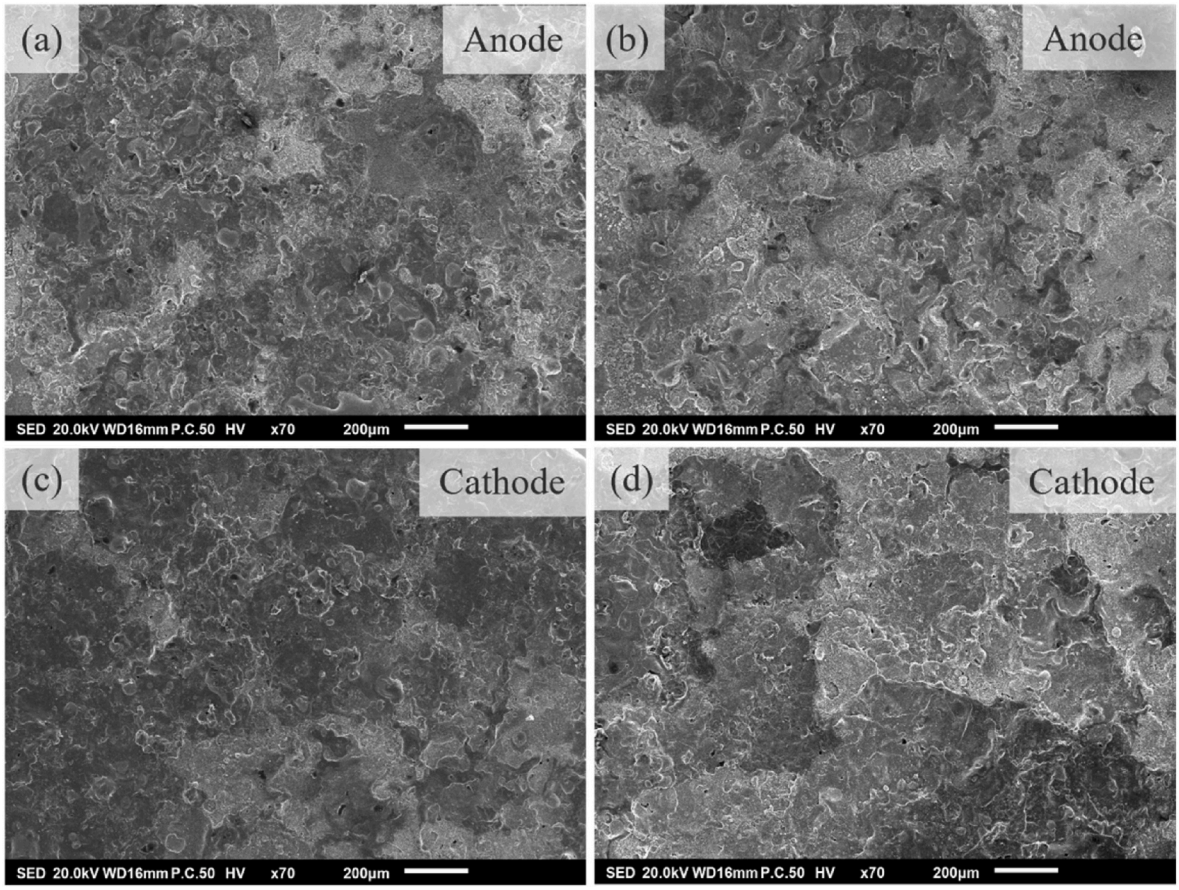

Fig. 12. SEM images after erosion with 30 V DC, 30 A: (a, c) Al_2O_3–Cu/30Cr; (b, d) 0.3GO-0.3Ag/Al_2O_3–Cu/30Cr.

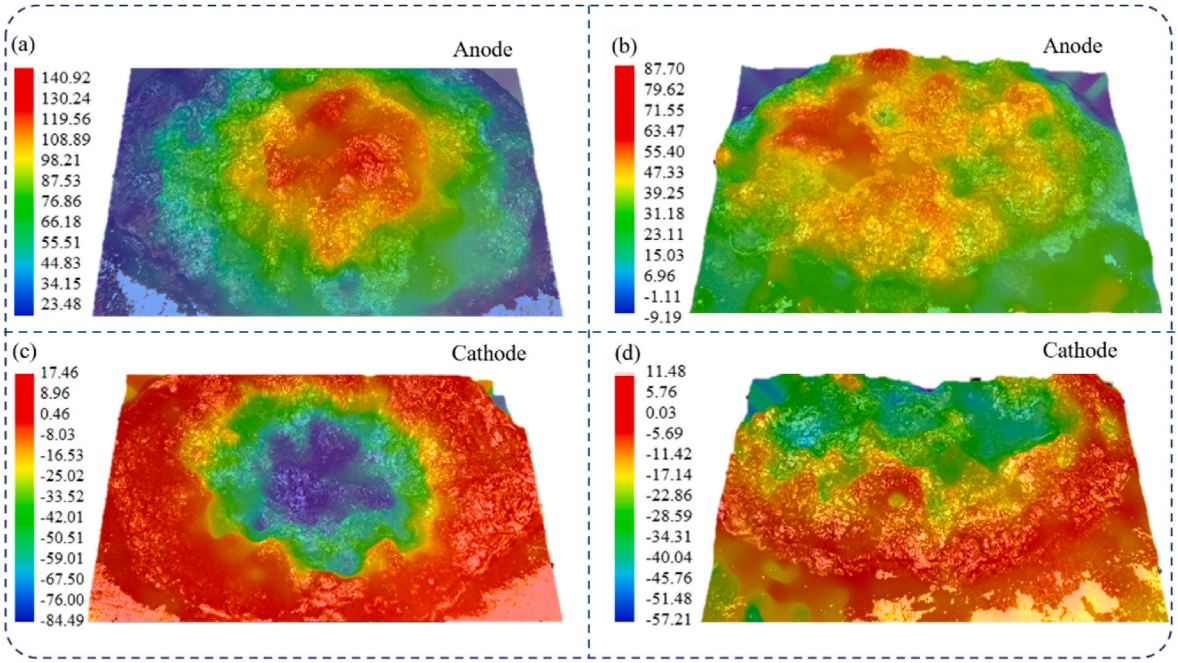

Fig. 13. Three-dimensional images after 30 V DC, 30 A erosion:(a, c) Al_2O_3–Cu/30Cr; (b, d) 0.3GO-0.3Ag/Al_2O_3–Cu/30Cr.

$$4Cr + 3O_2 = 2Cr_2O_3 \quad (6)$$

In the equation, chromium oxidation generates Cr_2O_3 at high temperature. It is not easy to decompose, which means it has good high temperature stability. As the arc is extinguished, the heat of the melting zone is rapidly dissipated in the surrounding environment. However, the absorption of excess O_2 will not be immediately discharged. Hence the

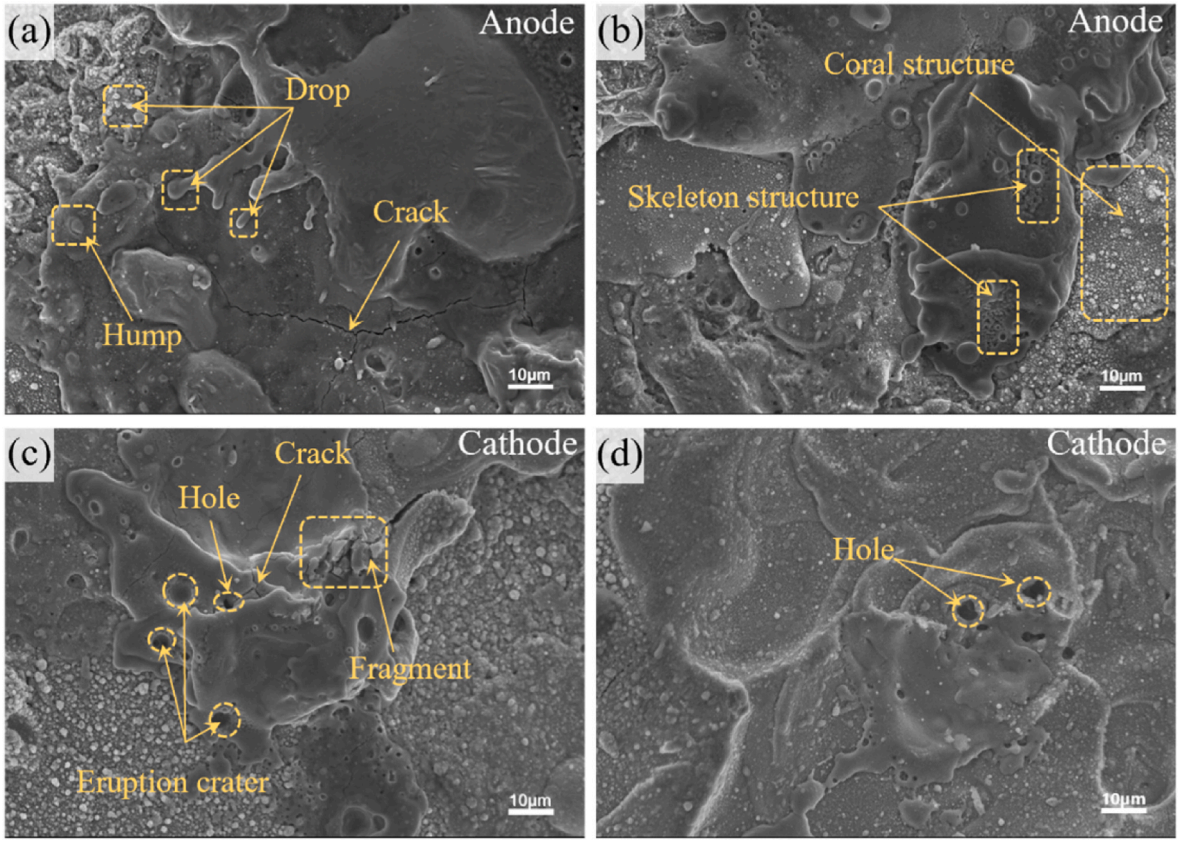

Fig. 14. SEM images after arc erosion: (a, c) Al_2O_3–Cu/30Cr; (b, d) 0.3GO-0.3Ag/Al_2O_3–Cu/30Cr.

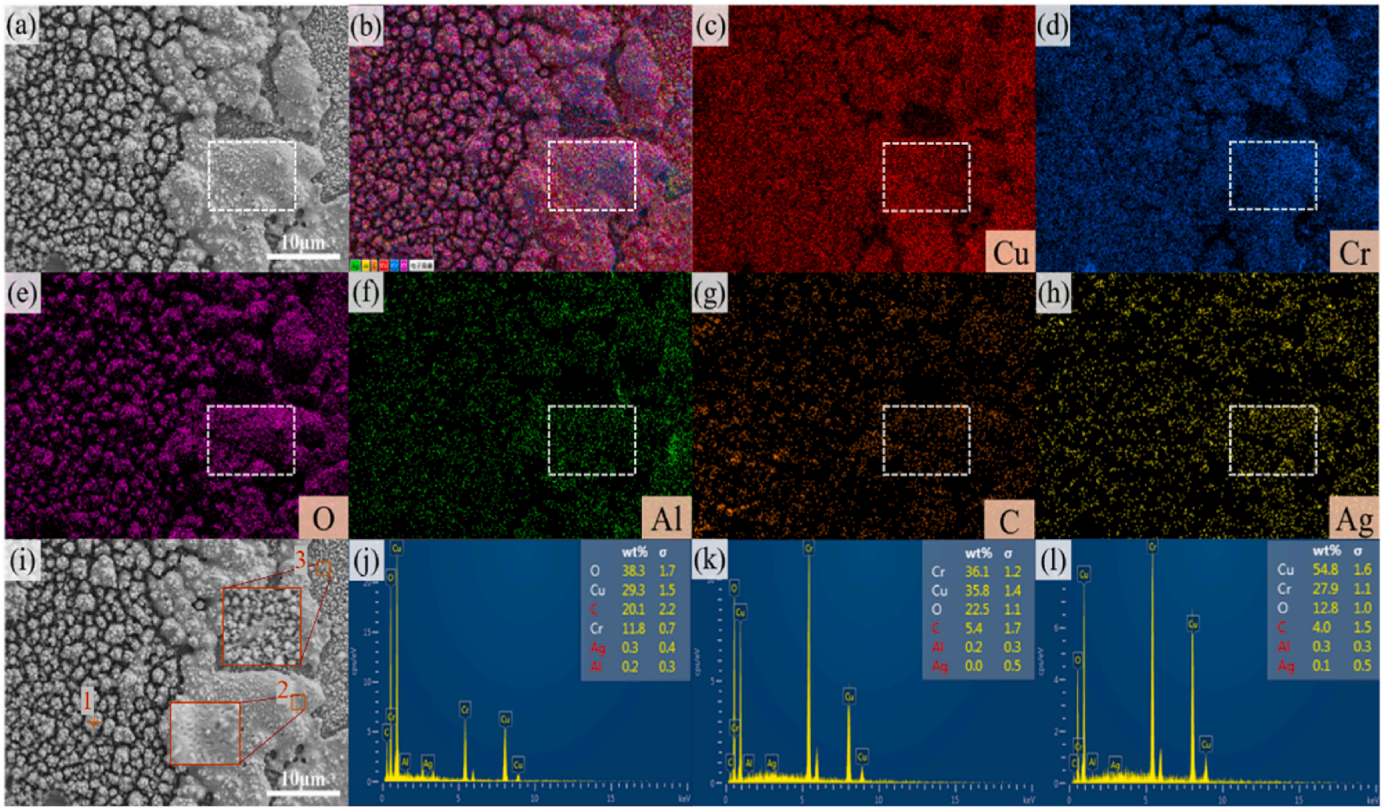

Fig. 15. SEM images and EDS results of the 0.3GO-0.3Ag/Al_2O_3–Cu/30Cr after erosion under 30 V DC, 30 A.

solid-liquid intersection of O_2 saturation is very high, and so on the contact cycle again to produce arc overheating, the region is prone to produce bubbles. In addition, depending on the viscosity of the molten metal, the gas escape rate and the pore size after the bubble rupture are different, and the shape of the formed pores varies. Such as pits, holes, etc., as shown in Fig. 14(c), where broken pieces are also clearly observed, this is because the porosity reduces the mechanical strength of the molten layer, which is highly susceptible to initiating cracks, which in turn lead to the formation of large cracks, resulting in the peeling of the surface layer of the material. Comparing with Fig. 14(d), the 0.3GO-0.3Ag/Al_2O_3–Cu/30Cr contact material has a small amount of porosity and it is difficult to find the gas eruption pits, which further proves that the incorporation of GO and Ag reduces the mass transfer and loss of the electrical contact material. Arc erosion morphology is the result of a variety of factors, and is closely related to the internal structure of the material, performance and external conditions of use. In summary, under the same electrical erosion conditions, the cracks, pits and other defects of the 0.3GO-0.3Ag/Al_2O_3–Cu/30Cr contact material are significantly less than those of the Al_2O_3–Cu/30Cr contact material, which further indicates that the addition of trace amounts of GO and Ag can improve the thermal stability of the contact material in order to extend the service life of the contacts.

Fig. 15 shows the SEM images and EDS results of the 0.3GO-0.3Ag/Al_2O_3–Cu/30Cr after erosion under 30 V DC, 30 A. The elements of the contact surface were mixed uniformly after the test, and at the same time, the oxygen content increased significantly. Due to the two contacts were in the conditions of air blowing argon, the high-density current to produce high-temperature arc result in the surface of the melting layer area, thus it will absorb the atmospheric oxygen and the matrix Cu elements oxidized to Cu_2O. It plays a role in the arc to achieve the redistribution of elements. From the point and area scans, it demonstrates that the coral-like shape is mainly formed by the oxidation of sputtered Cu droplets during the erosion process. Region 2 in Fig. 15 (i) is the skeleton structure, mainly Cr and O at high temperatures to generate Cr_2O_3 in the contact process under the action of gravity and adhesion slowly flow and combined to form a continuous distribution of the skeleton structure, the copper liquid will penetrate into the skeleton, thus inhibiting the flow of Cu and splashing to reduce the loss and transfer of materials [44]. It also reduces the soldering between the contacts and improves the breaking capacity between the two contacts. The added GO and Ag can improve the viscosity of the molten layer, which effectively reduce the flow of Cu, thus enabling the contacts to obtain superior electrical contact performance.

In order to further explore material transfer and failure mechanisms, the contact was cut longitudinally after the electrical erosion, then the sub-surface layer of the contact after the electrical erosion was observed, as shown in Fig. 16. From Fig. 16(a) and (c), it can be seen that the anode surface is partially covered by Cr, the cathode surface has obvious pits, vertical cracks and covered by Cr enhanced phase. What's more, elemental redistribution has occurred on cathode and anode surfaces. Thus, it was verified that the material was transferred from cathode to anode. Fig. 16(b) and (d) show an enlarged view of region 1 and 2, respectively, where many pores, vertical cracks and liquid droplets are clearly seen. The reason for this phenomenon is that the electrical contacts in the process of opening and closing, ionization between the contacts, arc discharge, the resulting arc heat makes the material melt at high temperatures, the contacts between the metal liquid-bridge will be generated. Under the influence of the combined factors of electron bombardment, electric field, and electromagnetic force plasma flow force of the high-energy arc. The cathode will emit electrons to the anode. And the cations will bombard the cathode surface, resulting in a higher density of heat flow on the cathode surface, which is much larger

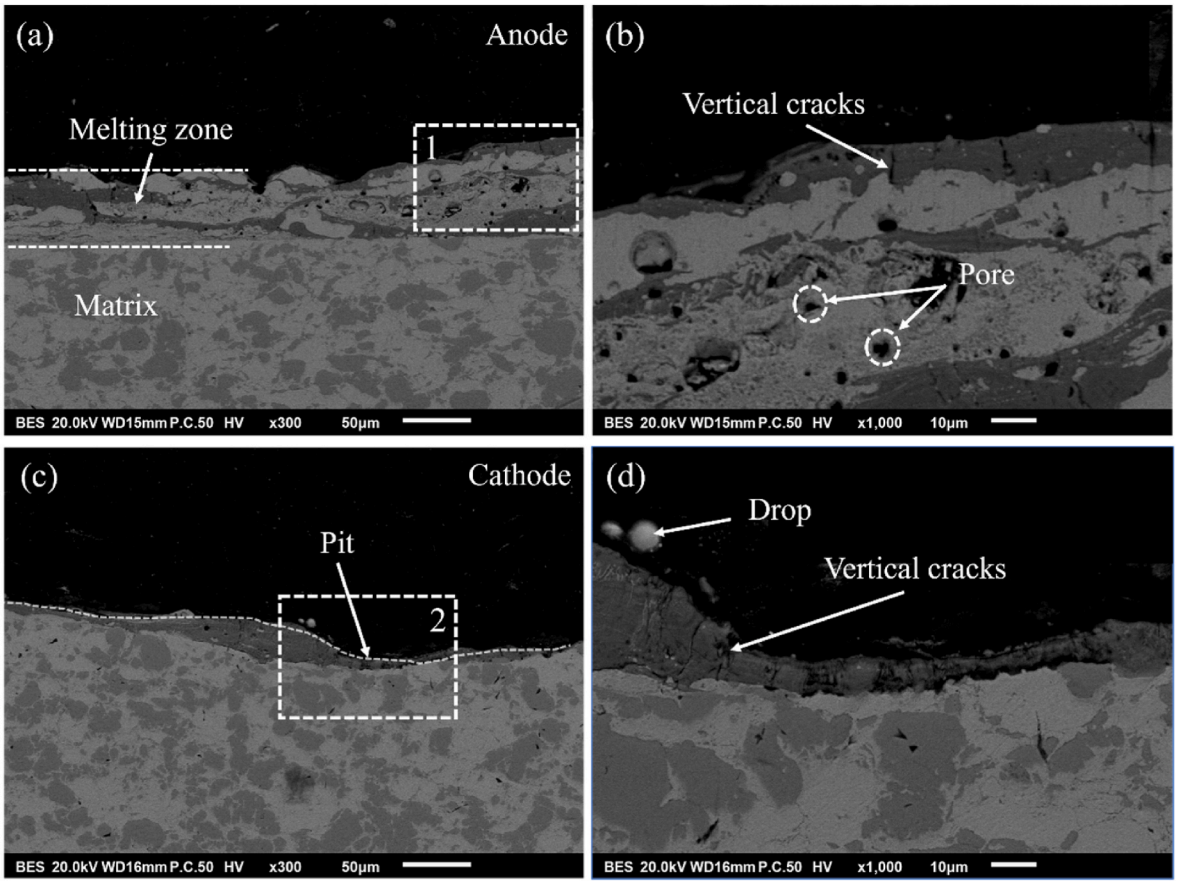

Fig. 16. Microscopic morphology of the sub-surface layer after erosion under 30 V DC, 30 A: (a)anode; (b) region 2 of (a); (c) cathode; (d) region 2 of (c).

than the anode heat [45,46]. The macroscopic manifestation is that the material on the surface of the cathode contact will be transferred to the surface of the anode with the liquid bridge as well as sputtered to the environment during the contact process, resulting in a pitted surface of the cathode contact and a raised surface of the anode. Due to the existence of a huge heat flow density during the ignition arc, the metal surface is expanded by thermal stress. While absorbing a large amount of oxygen, the anode is transferred to the material melted at high temperature with mobility. After the arc is extinguished as the temperature decreases, the material shrinks, the surface of the fast-cooling will produce cracks. The subsurface of the excess gas can't escape immediately, with the result that there are holes in the subsurface layer. And the stomatal holes are basically distributed in the Cu-rich area, as shown in Fig. 16(b). Defects such as porosity and cracks are important factors in the failure of contact materials.

4.3. Micro-strengthening mechanism

To investigate the micro-strengthening mechanism of the composite materials, a detailed analysis of their microstructure was conducted. Firstly, TEM analysis was performed on the 0.3GO-0.3Ag/Al_2O_3–Cu/30Cr composites. Fig. 17(a) shows the EDS results of Cr-containing particles, it can be seen that the Cr element is consistent with the signal of the O element, and the Al element is uniformly distributed in the Cu matrix with aggregation around the Cr element. In addition, the C element is mainly distributed at the interface, and the Ag is mainly in the Cu matrix. According to the phase diagram of Cu–Ag system [47], the equilibrium temperature of L(Ag) + (Cu) eutectic is 781 °C, and the maximum solubility of Ag in Cu is 3.1 wt %. Because the sintering temperature of this test is 950 °C, and the content of Ag is 0.3 wt %, so that the Ag is completely dissolved in the Cu matrix.

Fig. 18(a) shows that large number of dislocation tangles within the material, which significantly improves the mechanical properties of the composite. The black region in Fig. 18(b) is Cr particles, and its selected electron diffraction is shown in Fig. 18(c). Combined with Fig. 17(b), it can be determined that the gray region is the Cu matrix. And it can be seen that there are many γ-Al_2O_3 nanoparticles diffusely distributed on the Cu matrix, which can pin dislocations, impede the movement of grain boundaries, as well as playing a role in the diffusion strengthening. Combined with Fig. 18(d–f), it can be seen that the Cr–C compound Cr_3C_2 is generated at the interface of Cu and Cr, which nails the interface and is a ceramic compound with extremely high hardness and high temperature stability. Furthermore, it can act transmitting force against the force between Cu and Cr, resulting in scattering and absorbing the thermal shock. And improving the composite's mechanical properties and thermal stability.

In the Cr–C reaction, there are three possible reactions [48–50].

$$3Cr + 2C = Cr_3C_2,\ \Delta G = -58857 - 22.34T \quad (7)$$

$$7Cr + 3C = Cr_7C_3,\ \Delta G = -92067 - 41.5T \quad (8)$$

$$23Cr + 6C = Cr_{23}C_6,\ \Delta G = -236331 - 86.7T \quad (9)$$

where T (K) is the reaction temperature and ΔG (KJ/mol) is the Gibbs free energy. When the hot press sintering temperature is 1223 K, the Gibbs free energies of Cr_3C_2, Cr_7C_3, and $Cr_{23}C_6$ are generated as −87.18 kJ/mol, −142.8 kJ/mol, and −342.36 kJ/mol, respectively, and the Gibbs free energies are less than zero, and the stability $Cr_{23}C_6 > Cr_7C_3 > Cr_3C_2$. Fig. 18(d) is the high resolution of region 2 in Fig. 18(b), which shows that there is an interfacial reaction layer at the boundary, and Cr_3C_2 is generated between the Cu matrix and the reinforcing phase Cr particles. Fig. 18(e) is a HRTEM enlarged image of area 3 in Fig. 18(d), and its FFT is shown in Fig. 18(g). Fig. 18(d) shows the diffraction spots of 4. Since the γ-Al_2O_3 particles in the Cu matrix are small, the image after FFT transformation is fuzzy, and only the diffraction spots of Cu can be accurately provided here. Through TEM analysis, the good micro-interface improved the electrical contact properties of the composites and helped to improve the compression properties.

5. Conclusion

(1) Al_2O_3–Cu/30Cr and 0.3GO-0.3Ag/Al_2O_3–Cu/30Cr composites were prepared by rapid hot-press sintering internal oxidation method. Their relative densities are greater than 99%. The compressive strength and hardness of the 0.3GO-0.3Ag/Al_2O_3–Cu/30Cr composite increased by 2.6% and 7.3%. The thermal conductivity is increased by 51.6% at 150 °C.

(2) The incorporation of GO and Ag reduced mass transfer and loss in the electrical contact materials. At a current of 30 A, the 0.3GO-0.3Ag/Al_2O_3–Cu/30Cr composite exhibited reductions of 34.3% in anodic increase, 38.3% in cathodic decrease, and 54.8% in mass loss compared to the Al_2O_3–Cu/30Cr composite.

(3) The mass transfer from cathode to anode was observed in Al_2O_3–Cu/30Cr and 0.3GO-0.3Ag/Al_2O_3–Cu/30Cr. After arc erosion, the cathode surface was almost completely covered with Cr-enhanced phases featuring vertical cracks, while the anode surface showed localized coverage of Cr, indicating elemental redistribution at both electrodes.

(4) Chromium-carbon compounds Cr_3C_2 were generated at the Cu–Cr interface, enhanced the overall performance of the composites.

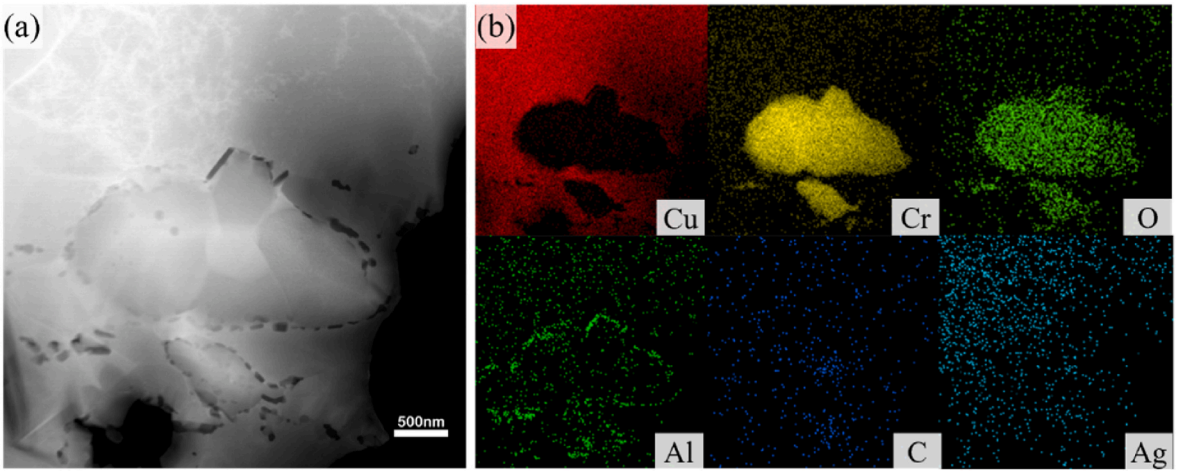

Fig. 17. EDS results of the 0.3GO-0.3Ag/Al_2O_3–Cu/30Cr composites containing Cr particles.

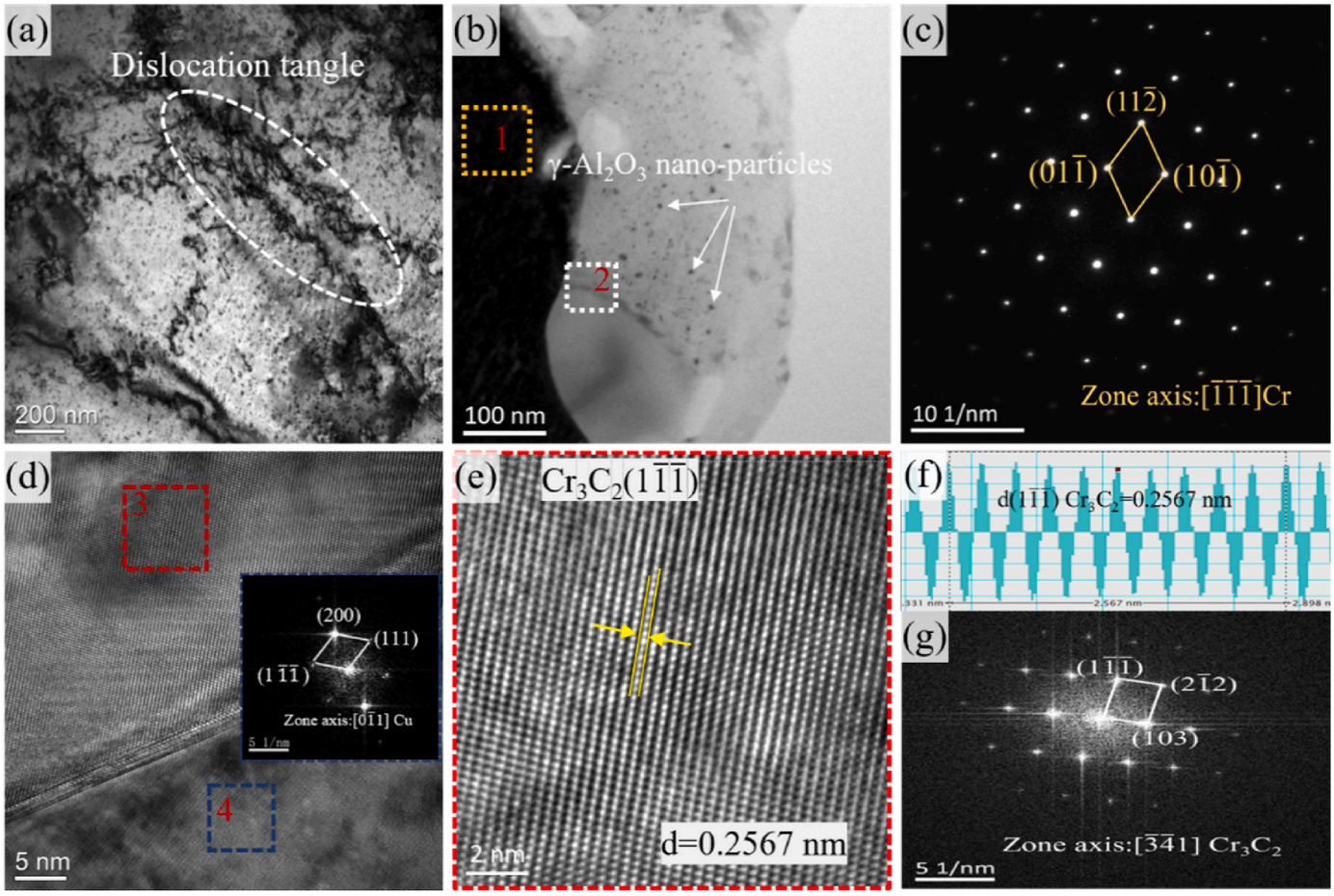

Fig. 18. TEM images of the 0.3GO-0.3Ag/Al_2O_3–Cu/30Cr composite: (a, b) Bright-field images of the composite; (c) SAED of region 1 in (b) (d) HRTEM of region 2 in (b); (e) HRTEM of region 3 in (d); (f) Crystal plane spacing of Cr_3C_2 of (e); (g) FFT of (e)

Data availability

The data that has been used is confidential.

Declaration of competing interest

The authors declare that they have no known competing financial interests or personal relationships that could have appeared to influence the work reported in this paper.

Acknowledgments

This work was supported by the National Natural Science Foundation of China (52071134, 52374367), the Program for Innovative Research Team at the University of the Henan Province (22IRTSTHN001), Leading Talents of Science and Technology in the Central Plain of China (244200510029), the Joint Foundation for Science and Technology Research and Development Plan of Henan Province (232103810030, 232103810031), Key Research and Development Program of Henan Province (231111232000, 231111231300).

References

[1] Novak P, Benediktova D, Mestek S, Tsepeleva A, Kopecek J. Aluminum alloys with natural ratio of alloying elements manufactured by powder metallurgy. J Alloys Compd 2022;931:167440. https://doi.org/10.1016/j.jallcom.2022.167440.
[2] Abhishek P, Vimal E, Abhishek BM, Chandra SP, Rajneesh H, Satish VK. In-situ interfacial growth of TiAl intermetallic and its influence on microparticle dislodgement during abrasive wear of Al/Ti6Al4V composite. Mater Today Commun 2020;24:101123. https://doi.org/10.1016/j.mtcomm.2020.101123.
[3] Canakci A, Varol T, Cuvalci H, Erdemir F, Ozkaya S, Yalcın ED. Synthesis of novel $CuSn_{10}$-graphite nanocomposite powders by mechanical alloying. Micro & Nano Lett 2014;9:109–12. https://doi.org/10.1049/mnl.2013.0715.
[4] Varol T, Güler O, Akçay SB, Aksa HC. The effect of silver coated copper particle content on the properties of novel Cu-Ag alloys prepared by hot pressing method. Powder Technol 2021;384:236–46. https://doi.org/10.1016/j.powtec.2021.02.020.
[5] Zhang XX, Yuan YL, Zhao SQ, Zhang J, Yan QZ. Microstructure stability, softening temperature and strengthening mechanism of pure copper, CuCrZr and Cu-Al_2O_3 up to 1000 °C. Nucl Mater 2022;30:101123. https://doi.org/10.1016/j.nme.2022.101123.
[6] Sadoun AM, Fathy A. Experimental study on tribological properties of Cu-Al_2O_3 nanocomposite hybridized by graphene nanoplatelets. Ceram Int 2019;45(18):24784–92. https://doi.org/10.1016/j.ceramint.2019.08.220.
[7] Abd-Elaziem W, Hamada A, Allam T, Mohammed MM, Abd-El Hamid M, Samah S, et al. Enhancement of mechanical and physical properties of Cu–Ni composites by various contents of Y_2O_3 reinforcement. J Mater Res Technol 2024;30:473–84. https://doi.org/10.1016/j.jmrt.2024.03.075.
[8] Bera S, Manna I. Synthesis of CuCr and CuCrAg alloy with nano-ceramic dispersion by mechanical alloying and consolidation by laser assisted sintering. Mater Chem Phys 2012;132(1):109–18. https://doi.org/10.1016/j.matchemphys.2011.11.005.
[9] Fathy A, Elkady O, Abu-Oqail A. Microstructure, mechanical and wear properties of Cu-ZrO_2 nanocomposites. Mater Sci Technol 2017;233(17):2138–46. https://doi.org/10.1080/02670836.2017.1353668.
[10] Fathy A. Investigation on microstructure and properties of Cu-ZrO_2 nanocomposites synthesized by in situ processing. Mater Lett 2018;213:95–9. https://doi.org/10.1016/j.matlet.2017.11.023.
[11] Guo XH, Song KX, Liang SH, Wang X, Zhang YM. Effect of Al_2O_3 particle size on electrical wear performance of Al_2O_3/Cu composites. Tribol Trans 2016;59:170–7. https://doi.org/10.1080/10402004.2015.1061079.
[12] Tian BH, Liu P, Song KX, Li Y, Liu Y, Ren FZ, et al. Microstructure and properties at elevated temperature of a nano-Al_2O_3 particles dispersion-strengthened copper base composite. Mater Sci Eng, A 2006;435–436:705–10. https://doi.org/10.1016/j.msea.2006.07.129.
[13] Varol T, Canakci A. The effect of type and ratio of reinforcement on the synthesis and characterization Cu-based nanocomposites by flake powder metallurgy.

J Alloys Compd 2015;649:1066–74. https://doi.org/10.1016/j.jallcom.2015.07.008.
[14] Luo HB, Sui YW, Qi JQ, Meng QK, Wei FX, He YZ. Copper matrix composites enhanced by silver/reduced graphene oxide hybrids. Mater Lett 2017;196:354–7. https://doi.org/10.1016/j.matlet.2017.03.084.
[15] Chu K, Wang F, Li YB, Wang XH, Huang DJ, Zhang H. Interface structure and strengthening behavior of graphene/CuCr composites. Carbon 2018;133:127–39. https://doi.org/10.1016/j.carbon.2018.03.018.
[16] Nazeer F, Ma Z, Gao LH, Abrar S, Malik A, Khan MA, et al. Higher mechanical and thermal properties of Cu-rGO composites. Vacuum 2020;180:109584. https://doi.org/10.1016/j.vacuum.2020.109584.
[17] Bodrova LE, Melchakov SY, Shubin AB, Goyda EY. Smart-microstructures of composites forelectrical contacts with frameless packing of Cr and W in copper. T Nonferr Metal Soc 2021;31(9):2773–86. https://doi.org/10.1016/S1003-6326(21)65692-3.
[18] Shu SC, Zhang Q, Ihde J, Yuan QL, Dai W, Wu ML, et al. Surface modification on copper particles toward graphene reinforced copper matrix composites for electrical engineering application. J Alloys Compd 2022;891:162058. https://doi.org/10.1016/j.jallcom.2021.162058.
[19] Li H, Zhou M, Tian BH, Zhang Y, Ma ZP, Li X, et al. Microstructure and electrical contact properties of Al_2O_3-Cu/(Cr, Zr) composites. Mater Today Commun 2024;38:107747. https://doi.org/10.1016/j.mtcomm.2023.107747.
[20] Wu Q, Xu GF, Yuan M, Wu CP. Influence of operation numbers on arc erosion of Ag/CdO electrical contact materials. IEEE Trans Compon Packag Manuf 2020;10(5):845–57. https://doi.org/10.1109/TCPMT.2020.2971627.
[21] Li WJ, Chen ZY, Jiang H, Sui XH, Zhao CF, Zhen L, et al. Effects of interfacial wettability on arc erosion behavior of Zn_2SnO_4/Cu electrical contacts. J Mater Sci Technol 2022;109:64–75. https://doi.org/10.1016/j.jmst.2021.08.045.
[22] Cui R, Han Y, Zhu ZX, Chen BA, Ding Y, Zhang Q, et al. Investigation of the structure and properties of electrodeposited Cu/graphene composite coatings for the electrical contact materials of an ultrahigh voltage circuit breaker. J Alloys Compd 2019;777:1159–67. https://doi.org/10.1016/j.jallcom.2018.11.096.
[23] Robert F. Prediction of contact length, contact pressure and indentation depth of Au/carbon nanotube composite micro electrical contact using finite element modeling. Appl Surf Sci 2019;489:470–6. https://doi.org/10.1016/j.apsusc.2019.05.169.
[24] Lin ZJ, Gao WH, Li SY, Shen Q, Dai PQ, Zou LC, et al. Effect of in-situ phase transition of (MgCoNiCuZn)O high-entropy oxides on microstructure and performance of Ag-based electrical contact materials. Appl Surf Sci 2023;630:157479. https://doi.org/10.1016/j.apsusc.2023.157479.
[25] Wang XR, Wei SZ, Xu LJ, Fang F, Li JW, Pan KM, et al. Effect of sintering temperature on fine-grained Cu-W composites with high copper. Mater Char 2019;153:121–7. https://doi.org/10.1016/j.matchar.2019.04.017.
[26] Zygmuntowicz J, Los J, Kurowski B, Piotrkiewicz P, Kaszuwara W. Investigation of microstructure and selected properties of Al_2O_3-Cu and Al_2O_3-Cu-Mo composites. Adv Compos Hybrid Mater 2021;4:212–22. https://doi.org/10.1007/s42114-020-00188-8.
[27] Zhang XH, Zhang Y, Tian BH, An JC, Zhao Z, Volinsky AA, et al. Arc erosion behavior of the Al_2O_3-Cu/(W, Cr) electrical contacts. Composites Part B 2019;160:110–8. https://doi.org/10.1016/j.compositesb.2018.10.040.
[28] Gong TM, Yao PP, Xiong X, Zhou HB, Zhang ZY, Xiao YL, et al. Microstructure and tribological behavior of interfaces in Cu-SiO_2 and Cu-Cr metal matrix composites. J Alloys Compd 2019;786:975–85. https://doi.org/10.1016/j.jallcom.2019.01.255.
[29] Lin RJ, Wang LJ, Ma JW, Shi WX, Deng J, Jia SL. Experiment investigation on vacuum arc of AMF contacts under different materials. AIP Adv 2018;8(9):095110. https://doi.org/10.1063/1.5047505.
[30] Inada Y, Kikuchi R, Nagai H, Kumada A, Hidaka K, Maeyama M. Influence of CuCr electrode composition on 2D electron and metal vapor density distribution over vacuum arc. J Phys D Appl Phys 2020;53:305201. https://doi.org/10.1088/1361-6463/ab83bd.
[31] Papillon A, Roure S, Schellekens H, Missiaen JM, Chaix JM, Rigal E. Investigation on the chemical reactions affecting the sinterability and oxide content of Cu-Cr composites during the solid state sinteringprocess. Mater Des 2017;113:353–60. https://doi.org/10.1016/j.matdes.2016.09.038.
[32] Zhu HJ, Tian BH, Zhang Y, Zhou M, Li YZ, Zheng XH, et al. Microstructure and electrical contact behavior of the nano-yttria-modified Cu-Al_2O_3/30Mo/3SiC composite. Nanotechnol Rev 2023;12(1):20220532. https://doi.org/10.1515/ntrev-2022-0532.
[33] Güler O, Varol T, Alver Ü, Kaya G, Yıldız F. Microstructure and wear characterization of Al_2O_3 reinforced silver coated copper matrix composites by electroless plating and hot pressing methods. Mater Today Commun 2021;27:102205. https://doi.org/10.1016/j.mtcomm.2021.102205.
[34] Güler O, Varol T, Alver Ü, Canakci A. Effect of Al_2O_3 content and milling time on the properties of silver coated Cu matrix composites fabricated by electroless plating and hot pressing. Mater Today Commun 2020;24:101153. https://doi.org/10.1016/j.mtcomm.2020.101153.
[35] Ma CJ, Li N, Gao H, Ding JX. Effect of Ag addition on the microstructure and electrical properties of $Ni_{0.6}CoMn_{1.4}O_4$/Ag composite ceramics. J Alloys Compd 2022;900:163528. https://doi.org/10.1016/j.jallcom.2021.163528.
[36] Zhou XY, Yi DQ, Nyborg L, Hu Z, Huang J, Cao Y. Influence of Ag addition on the microstructure and properties of copper-alumina composites prepared by internal oxidation. J Alloys Compd 2017;722:962–9. https://doi.org/10.1016/j.jallcom.2017.06.176.
[37] Li GB, Sun JB, Guo QM, Wang R. Fabrication of the nanometer Al_2O_3/Cu composite by internal oxidation. J Mater 2005;170(1–2):336–40. https://doi.org/10.1016/j.jmatprotec.2005.05.011.
[38] Wang J, Guo LN, Lin WM, Chu XD, Chen J, Zhang S, et al. The effects of graphene content on the corrosion resistance, and electrical, thermal and mechanical properties of graphene/copper composites. N Carbon Mater 2019;34(2):161–9. https://doi.org/10.1016/s1872-5805(19)60009-0.
[39] Akbari A, Cunning BV, Joshi SR, Wang CH, Camacho-Mojica DC, Chatterjee S, et al. Highly ordered and Dense thermally conductive graphitic films from a graphene oxide/reduced graphene oxide mixture. J Mat 2020;2(5):1198–206. https://doi.org/10.1016/j.matt.2020.02.014.
[40] Balandin AA, Ghosh S, Bao WZ, Calizo I, Teweldebrhan D, Miao F, et al. Superior thermal conductivity of single-layer graphene. Nano Lett 2008;8(3):902–7. https://doi.org/10.1021/nl0731872.
[41] Ding JX, Tian WB, Zhang PG, Zhang M, Chen J, Zhang YM, et al. Preparation and arc erosion properties of Ag/Ti_2SnC composites under electric arc discharging. J Adv Ceram 2019;8:90–101. https://doi.org/10.1007/s40145-018-0296-y.
[42] Guo XH, Yang YB, Song KX, Li SL, Jiang F, Wang X. Arc erosion resistance of hybrid copper matrix composites reinforced with CNTs and micro-TiB_2 particles. J Mater Res Technol 2021;11:1469–79. https://doi.org/10.1016/j.jmrt.2021.01.084.
[43] Cortazar-Martínez O, Torres-Ochoa JA, Raboño-Borbolla JG, Herrera-Gomez A. Oxidation mechanism of metallic chromium at room temperature. Appl Surf Sci 2021;542:148636. https://doi.org/10.1016/j.apsusc.2020.148636.
[44] Ma ZP, Zhou M, Li H, Jing K, Zhang JC, Tian BH, et al. Effects of Y_2O_3 on the hot deformation behavior and microstructure evolution of Al_2O_3-Cu/35Cr3TiB_2 electrical contact composites. Mater Char 2024;215:114120. https://doi.org/10.1016/j.matchar.2024.114120.
[45] Wu CP, Yi DQ, Weng W, Li SH, Zhou JM. Influence of alloy components on arc erosion morphology of Ag/MeO electrical contact materials. T Nonferrous Met Soc 2016;26(1):185–95. https://doi.org/10.1016/s1003-6326(16)64105-5.
[46] Xi Y, Wang XH, Zhou ZJ, Li HY, Guo XH. Material transfer behavior of $AgTiB_2$ contact under different contact forces and electrode gaps. T Nonferrous Met Soc 2019;29(5):1046–56. https://doi.org/10.1016/S1003-6326(19)65013-2.
[47] Subramanian PR, Perepezko JH. The ag-cu (silver-copper) system. JPE 2007;14:62–75. https://doi.org/10.1007/BF02652162.
[48] Sichen D, Sheetharaman S, Staffansson L-I. Standard Gibbs energies of formation of the carbides of chromium by emf measurements. Metall Trans B 1988;19:951–7. https://doi.org/10.1007/BF02651418.
[49] Teng LD, Lu KG, Aune RE, Seetharaman S. Thermodynamic investigations of Cr_3C_2 and reassessment of the Cr-C system. Metall Mater Trans A 2004;35:3673–80. https://doi.org/10.1007/s11661-004-0273-7.
[50] Chu K, Wang F, Li YB, Wang XH, Huang DJ, Zhang H. Interface structure and strengthening behavior of graphene/CuCr composites. Carbon 2018;133:127–39. https://doi.org/10.1016/j.carbon.2018.03.018.